Charge and Photoionization Properties of Single Semiconductor Nanocrystals

ARTICLE *in* THE JOURNAL OF PHYSICAL CHEMISTRY B · FEBRUARY 2001

Impact Factor: 3.3 · DOI: 10.1021/jp0023415

3 AUTHORS, INCLUDING:

Todd D Krauss
University of Rochester
119 PUBLICATIONS **5,455** CITATIONS
SEE PROFILE

Stephen O'Brien
City College of New York
126 PUBLICATIONS **7,788** CITATIONS
SEE PROFILE

Charge and Photoionization Properties of Single Semiconductor Nanocrystals

Todd D. Krauss,[†] Stephen O'Brien,[‡] and Louis E. Brus*

Department of Chemistry, Columbia University, New York, New York 10027

Received: June 30, 2000; In Final Form: December 1, 2000

The electrostatic charge and photoionization characteristics of 5-nm CdSe nanocrystals were directly observed with electrostatic force microscopy (EFM) in dry air at room temperature. Measurements were made on individual nanocrystals, as well as on those in self-assembled rafts. Nanocrystals are initially charge neutral if protected from sources of light. However, over a few weeks some nanocrystals develop a single positive charge if exposed to ambient light. The determination of the charge magnitude per nanocrystal within the framework of EFM theory is described. EFM measurements with simultaneous above band gap laser photoexcitation provide direct evidence of nanocrystal photoionization. A small percentage of photoionized nanocrystals exhibit a blinking behavior in their charge. The linear dependence of nanocrystal photoionization rates on excitation intensity indicates that the ionization process occurs via a single photon. EFM measurements of core/shell CdSe nanocrystals show that photoionization is slower in the presence of an electron barrier at the nanocrystal surface. Photoionization and subsequent neutralization are quantitatively modeled with a two-level system.

Introduction

Semiconductor nanocrystals have been the subject of much interest over the past decade due to their remarkable physical properties and potential for use in numerous areas. (For a recent review, see refs 1 and 2.) While the optical and electronic properties of semiconductor nanocrystals are partially understood, the electrostatic properties of semiconductor nanocrystals have received little attention. These properties are important because nanocrystals that have an electrostatic charge will have very different optical and electronic properties from nanocrystals without a charge. Optical selection rules, oscillator strengths, electron−phonon coupling, charge carrier lifetimes, and electron transport properties are all significantly affected by the presence of charges on a nanocrystal.

In the simplest picture, CdSe nanocrystals are expected to have a permanent dipole moment that scales with the size of the nanocrystal. This is because bulk CdSe crystallizes in the wurtzite structure, which has a structural dipole moment along the *c*-axis. More sophisticated theoretical treatments show that the dipole moment of a nanocrystal depends critically on surface reconstruction and stoichiometry, in addition to the nanocrystal radius.[3] Recently, the dipole moments of an ensemble of CdSe nanocrystals were measured as a function of nanocrystal size.[4] Here it was proposed that the origin of the dipole moment was not structural but due to thermal population of surface states in a neutral nanocrystal.

Other studies also imply the presence of internal electric fields in CdSe nanocrystals resulting from either charges and/or dipole moments. Investigations of exciton−phonon coupling,[5] two-photon fluorescence excitation,[6] and Raman spectroscopy[7] all suggest that, on average, CdSe nanocrystals have permanent internal electric fields. The presence of local electric fields from trapped charges was also inferred from quantum-confined Stark effect measurements.[8,9] These studies illustrate the importance of direct measurements of the electrostatic properties of individual CdSe nanocrystals.

In 1996, the photoluminescence of single CdSe nanocrystals was reported to exhibit a remarkable "on−off" or blinking behavior.[10,11] The photoluminescence blinking was postulated to arise from an Auger ionization and subsequent neutralization of the nanocrystal.[10,12] However, the nature of the ionized state and the ionization process are still not understood.[9] Auger ionization might also explain the photoluminescence intermittency observed in other nanoparticle systems such as InP,[13] porous Si,[14] and GaAs.[15] Direct measurements of the charge per nanocrystal with simultaneous photoexcitation provide a strategy with which to definitively answer these questions.

Here we present direct measurements of single electrostatic charges on individual CdSe nanocrystals with and without photoexcitation. CdSe nanocrystals ∼5 nm in diameter, with organic and inorganic surface passivation, were studied with electrostatic force microscopy (EFM) in dry air at 300 K. We determine that CdSe nanocrystals as prepared with standard methods are charge neutral. However, these nanocrystals slowly develop a permanent positive elementary charge upon extended exposure to weak, ambient light. EFM measurements taken during photoexcitation show photoionization of individual nanocrystals. The probability of a given nanocrystal photoionizing is proportional to the product of excitation intensity and exposure time. Measurements of the average ionization time as a function of excitation intensity suggest that ionization occurs via a single photon, with a probability of $\sim 5 \times 10^{-6}$ per excitation. Studies of nanocrystals with varying surface passivation indicate that ionization results from the photoexcited electron tunneling out the core of the nanocrystal and into its surroundings. Preliminary results have been previously reported.[16]

EFM Theory. Electrostatic force microscopy measures the long-range electrostatic attraction between a conductive atomic

[†] Present address: Department of Chemistry, University of Rochester, Rochester, NY 14627.

[‡] Present address: Department of Applied Physics, Columbia University, New York, NY, 10027.

10.1021/jp0023415 CCC: $20.00
Published on Web 02/07/2001

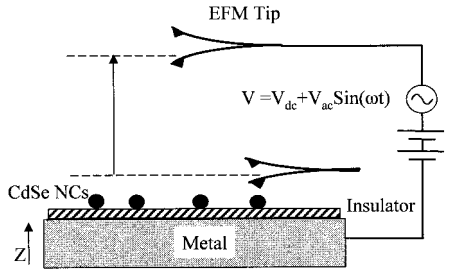

Figure 1. Schematic of the typical experimental setup for EFM. CdSe nanocrystals are modeled as having a fixed charge Q.

force microscope (AFM) cantilever and a conductive substrate. A schematic of the experimental geometry for EFM is shown in Figure 1. The attractive force between the metallic EFM tip and the conductive substrate, resulting from the applied voltage, is treated as a capacitive interaction.[17,18] Any fixed charge, Q, is treated as a point charge located directly on the insulator surface. Surface charges generate image charges in the tip and in the metallic substrate. Surface charges, and their images, interact with the total charge on the EFM tip through a Coulombic interaction.[17,18]

The attraction between the cantilever and the substrate is proportional to the square of the voltage difference between them. Thus, application of a sinusoidal voltage, $V = V_{dc}+V_{ac}\sin(\omega t)$, yields components of the attractive force at zero frequency, ω and 2ω. By using lock-in detection techniques, we can select the components of the force on the tip at ω and 2ω, which are given by

$$F(\omega) = \left(\frac{\partial C}{\partial z}(V_{dc}+\phi) + \frac{QC}{4\pi\epsilon_0(z+R)^2} + \frac{Q_1 C}{4\pi\epsilon_0\left(z+R+\frac{2h}{\epsilon_1}\right)^2} + \frac{\partial C}{\partial z}\frac{Q_2}{C}\right)V_{ac} \quad (1)$$

and

$$F(2\omega) = \frac{\partial C}{\partial z}\frac{V_{ac}^{\,2}}{4} \quad (2)$$

The EFM tip is modeled as a sphere of radius R. C is the capacitance between the EFM tip and the metallic substrate, and z is the separation between the insulator surface and the bottom of the EFM tip. ϕ is the contact potential difference between the tip and the substrate and is given in a vacuum by $\phi = (W_{substrate} - W_{tip})/(-e)$. In the expression for ϕ, e is the electron charge, and $W_{substrate}$ (W_{tip}) is the work function of the substrate (tip). The insulator thickness is h with a dielectric constant ϵ_1. Q_1 and Q_2 are induced charges on the metallic substrate and the EFM tip, respectively. The last term in eq 1 represents the force on the tip (at ω) from Q_2. For modeling simplicity, we assumed a parallel plate geometry between the tip and the substrate, Q_1 and Q_2:

$$Q_1 = -Q\frac{z}{(h/\epsilon + z)} \quad (3)$$

and

$$Q_2 = -Q\left(1 - \frac{z}{(h/\epsilon + z)}\right) \quad (4)$$

By varying V_{dc} with respect to ϕ, the first term in eq 1 can be completely nulled out, thus determining the magnitude and sign of Q.[17,18] Expressions analogous to eqs 1−4 can also be obtained for static electric fields coming from permanent multipole moments.

Local dielectric properties, which influence dC/dz, can be determined by fitting the measured force on the cantilever at 2ω.[17,18] If a dielectric material is between the tip and the substrate, the applied ac voltage induces an ac dipole in the material. In the simplest approximation, this dipole is proportional to the volume of the material times the relative dielectric constant. The electric field of this ac dipole is observed in the force at 2ω.

Martin et al. first realized the ability of an oscillating AFM tip to probe extremely weak forces with nanometer spatial resolution in the lateral dimension.[19] An oscillating AFM tip can be modeled as a simple harmonic oscillator, with a quality factor $S \gg 1$. Force gradients normal to the sample surface modify the effective resonant frequency ν of the vibrating cantilever

$$\nu = \nu_o\sqrt{1 - \frac{1}{\kappa}\frac{\partial F}{\partial z}} \quad (5)$$

where κ is the cantilever spring constant. For $\Delta\nu = \nu - \nu_o \ll \nu$, the change in resonant frequency is

$$\Delta\nu = \frac{-\nu}{2\kappa}\frac{\partial F}{\partial z} \quad (6)$$

Relative changes in cantilever resonant frequency $\Delta\nu/\nu \sim 10^{-5}$ can be measured, corresponding to the electric field gradient about 10 nm from a point charge with magnitude about $^1/_{10}$ of an electron. The effective signal-to-noise ratio is limited by the time constant of the lock-in amplifier, which is itself limited by the data acquisition time per line scan. In converting the change in cantilever resonant frequency to a charge, significant sources of error include the uncertainty in the tip−substrate distance, the tip end radius, and the tip−substrate capacitance.

The above equations yield a qualitative understanding of the changes in cantilever resonant frequency $\Delta\nu(\omega)$ and $\Delta\nu(2\omega)$ as the EFM tip passes over a CdSe nanocrystal. For $\Delta\nu(2\omega)$, we expect an increase in the signal magnitude when over a nanocrystal due to the larger dielectric constant of the semiconductor nanocrystal ($\epsilon \sim 9$) compared to the surrounding air ($\epsilon \sim 1$). The $\Delta\nu(2\omega)$ signal increases because the capacitance, and hence its derivatives, increases when a dielectric is placed between the two electrodes. For $\Delta\nu(\omega)$ with V_{dc} set such that $V_{dc} + \phi = 0$, we expect to observe one of three types of behavior: an increase or decrease in the signal magnitude, corresponding to, respectively, a negatively or positively charged nanocrystal; and no observed change in signal magnitude, corresponding to a neutral nanocrystal.

If the sample contains no fixed charges, then EFM can be used to measure the capacitance of the tip−substrate system. The capacitance, and its derivatives with respect to z, must be known for an absolute determination of Q. Taking the derivative of eq 1 and inserting that result into eq 6, d^2C/dz^2 can be written as

$$\frac{\partial^2 C}{\partial z^2} = \frac{-2\kappa}{(V_{dc}+\phi)V_{ac}}\frac{\Delta\nu(\omega)}{\nu} \quad (7)$$

By holding V_{ac} and V_{dc} fixed and measuring $\Delta\nu(\omega)$ as a function

of z, we can obtain the capacitance between the EFM tip and the substrate by integrating eq 7 twice.

Experimental Section

A. Nanocrystal and Sample Preparation. Colloids of CdSe nanocrystals capped with trioctylphosphine oxide (TOPO) (see ref 20) and either one or six monolayers of ZnS (see refs 21 and 22) were prepared with established methods. The diameter of the CdSe nanocrystal core was ~5 nm. Nanocrystals were characterized by optical absorption spectroscopy and AFM. Sizes were obtained by comparing measured absorption spectra with the reported literature values.[20−22]

Highly luminescent CdSe/CdS core/shell nanocrystals capped with trioctylphosphine oxide/selenide (TOPO/TOPSe, 70:30) were synthesized according to a modified version of literature methods. The reaction consisted of a single-flask, two-injection synthesis based on techniques described by Murray et al.;[20] CdSe nanoparticles of ~4 nm diameter were prepared by injection of a trioctylphosphine (TOP) solution of $Cd(CH_3)_2$/TOPSe into TOPO at 300 °C. Provided favorable conditions of temperature, injection, and nanocrystal growth time were employed, size-selective precipitation was not necessary prior to the addition of the shell precursors. The solution was cooled to 180 °C and a second injection of a TOP solution of $Cd(CH_3)_2/[(CH_3)_3Si]_2S$ was initiated, corresponding in quantity to two monolayers of CdS around the CdSe nanoparticles. Heating to 200 °C for controlled periods of 10−30 min allowed epitaxial growth of CdS on the CdSe nanoparticle core. Peng et al. previously observed that $CdSe_xS_{x-1}$ alloys do not form during routine synthesis.[23] The absorption maximum shift from 535 nm (core) to 550 nm (core/shell),[21,22] the significant increase in photoluminescence quantum yield,[21,22] and the increase in size observed in TEM confirm that semiconductor capping occurred. Average nanoparticle diameter and size distribution were also determined from optical absorption spectroscopy. Comparisons with published optical absorption data correlated well with electron microscopy studies of size. The final average particle diameter was approximately 4.5 nm, deduced from optical absorption spectroscopy, TEM, and AFM.

Samples were prepared using one of two procedures. For single nanocrystal EFM measurements, dilute toluene solutions containing CdSe nanocrystals were spun onto a 1−5 nm thick insulator on a metallic substrate. Insulator−metal substrates consisted of SiO_2 on Si, a dodecanethiol self-assembled monolayer on Au, and poly(vinyl butyral) (PVB) spun on highly oriented pyrolytic graphite (HOPG). For measurements on self-assembled nanocrystal islands, ~30 μL of a dilute suspension of CdSe nanocrystals in hexane was dropped onto HOPG. Evaporation of the hexane allowed the nanocrystals to form 2-D assemblies on the HOPG.[24] To minimize the effects of airflow on the self-assembly of the nanocrystals, the HOPG was allowed to dry inside a sealed container.

B. EFM Procedures. AFM and EFM images were obtained at room temperature with a Nanoscope IIIa Multimode AFM inside a drybox with <3% relative humidity. EFM tips were commercial cobalt−chromium-coated Si cantilevers[25] with spring constants ranging from 1 to 5 N/m. To map the surface topographic and electrostatic properties simultaneously, the instrument was operated in an interleaved scanning mode such that each line scan comprised two passes. The first pass consisted of a tapping mode scan with no external voltage applied, obtaining the surface topography. The AFM tip was oscillated at its resonance frequency (60−90 kHz). Next, the tip was raised a fixed distance above the sample surface and scanned at that constant height with a voltage applied. Use of dual lock-in amplifiers enabled simultaneous measurements of $\Delta\nu(\omega)$ and $\Delta\nu(2\omega)$. Typical parameters were the following: $V_{ac} = 6$ V peak-to-peak, $\omega = 2\pi \times 800$ Hz, lock-in time constant $\tau = 3$ ms, scan rate = 1.25 Hz per line, and lift-height $z = 10-12$ nm. The acquisition time for a complete image was approximately 6 min. Images were recorded with $V_{dc} = -\phi$, and typically, $|V_{dc}| < 0.5$ V.

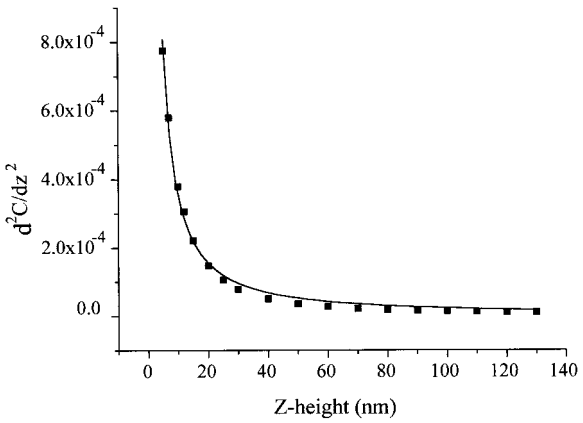

Figure 2. Graph of d^2C/dz^2 used to determine the tip−substrate capacitance. The solid symbols are the experimental data, and the line is a power-law fit. The sample consisted of freshly peeled HOPG.

For photoexcitation, continuous wave light from a HeCd laser ($\lambda = 442$ nm) or a diode laser ($\lambda = 780$) was coupled into the glovebox through an optical fiber and focused at grazing incidence onto the sample. Laser light was focused underneath the EFM tip with the use of a CCD camera and an optical microscope. When aligning the laser, low-intensity light was used ($I \sim 0.001$ W/cm^2) to avoid photoionization. For single nanocrystal measurements, excitation intensities were 20 W/cm^2, while for nanocrystal rafts, excitation intensities were typically 0.1−2 W/cm^2. Data acquisition consisted of first taking a background EFM scan to obtain the unexcited $\Delta\nu(\omega)$ (charge) image of the sample. Then, the sample was illuminated and the $\Delta\nu(\omega)$ image was recorded simultaneously. Consecutive images were recorded every 98 or 196 s for nanocrystal rafts or every 6 min for single nanocrystals. Images were recorded until the $\Delta\nu(\omega)$ signal remained unchanged for several consecutive images.

C. Determination of Charge Magnitude. As mentioned previously, accurate determination of charge and dielectric properties from the raw EFM images depends critically on the capacitance of the tip−substrate system and its derivatives with respect to z. This capacitance, and its dependence on z, is sensitive to the exact tip−sample geometry. To increase the accuracy in these values, we chose to measure the tip−substrate capacitance directly with EFM, in absence of any nanocrystals. The second derivative of the capacitance follows a power-law dependence $d^2C/dz^2 \sim z^{-1.4}$, as shown in Figure 2.[16] This value was remarkably consistent among all tips measured and implies that the capacitance lies between a sphere-plane ($d^2C/dz^2 \sim z^{-2}$), and a cone-plane ($d^2C/dz^2 \sim z^{-1}$) geometry.[26] Since the AFM tip shape is square-pyramidal, our measured value for d^2C/dz^2 seems reasonable.

The absolute magnitude of the charge, or permanent dipole moment, of a given nanocrystal was obtained from the EFM signal at $\Delta\nu(\omega)$. First, EFM images of $\Delta\nu(\omega)$ were recorded with $V_{dc} + \phi = 0$. Under this condition, the static electric field between the tip and substrate is zero, and image contrast arises only from sources of electric fields in the sample. While over

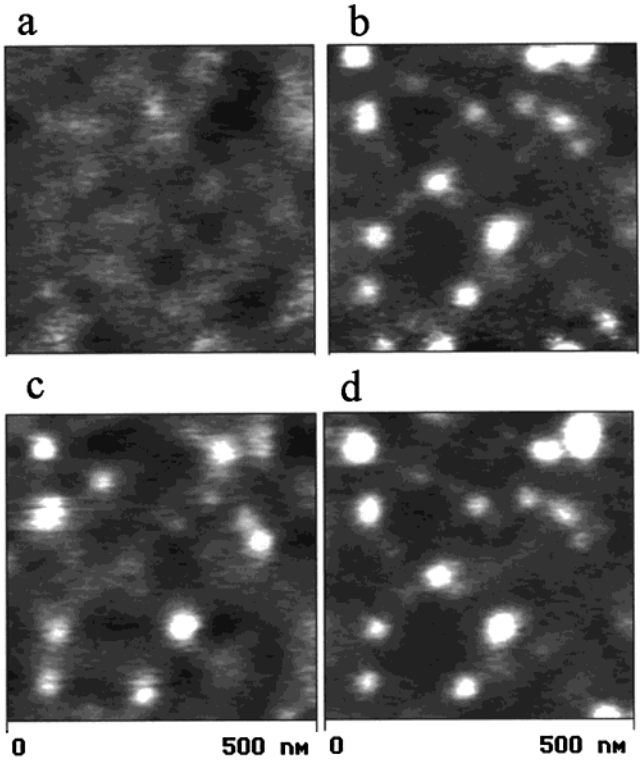

Figure 3. EFM (a) charge [$\Delta\nu(\omega)$] and (b) dielectric [$\Delta\nu(2\omega)$] image of CdSe nanocrystals capped with ZnS on 0.05% PVB spun coat from toluene, on a fresh surface of HOPG. EFM (c) charge and (d) dielectric image after reaching steady state from 442 nm photoexcitation at intensity 20 W/cm^2. The sign of $\Delta\nu(\omega)$ in parts a and c is inverted for clarity, such that bright portions of the image correspond to $\Delta\nu(\omega) < 0$.

a nanocrystal, V_{dc} was then adjusted such that the total $\Delta\nu(\omega)$ signal was identically zero. For an individual CdSe nanocrystal, typically, $\Delta\nu(\omega) = 0$ when $V_{dc} + \phi$ was ~80 mV and the lift height was 10 nm. Taking the derivative of eq 1 with respect to z, setting the result equal to zero, and inserting the measured value of $V_{dc} + \phi$ allows for an absolute determination of the charge magnitude provided the capacitance and its derivates are known.

Results and Discussion

A. Individual Nanocrystals without Laser Excitation. The charge image of semiconductor-capped CdSe nanocrystals on HOPG was initially quite different from that of TOPO-capped nanocrystals. Images of several hundred freshly synthesized CdSe nanocrystals, capped with ZnS, showed little or no contrast $\Delta\nu(\omega)$ as shown in Figure 3a. Images of CdSe nanocrystals, capped with CdS, also show little or no contrast in $\Delta\nu(\omega)$. The images were typically taken within 1 h of sample preparation. From the noise in the magnitude of $\Delta\nu(\omega)$, we conclude that the charge per nanocrystal must be $Q < 0.1e$. That is, the nanocrystals are neutral. Alternatively, the noise in $\Delta\nu(\omega)$ sets an upper limit of about 20 D for the z component of any permanent dipoles in these nanocrystals. Immediate images of several hundred TOPO-capped nanocrystals, which had been stored in similar organic solvents for several weeks in ambient light, show that about 50% of the nanocrystals exhibited a uniform $\Delta\nu(\omega)$ corresponding to a positive charge of absolute magnitude $Q \sim 0.5e$. The other 50% were neutral.[16]

The CdS- and ZnS-capped samples, stored in dry air under diffuse fluorescent lighting, did not remain neutral. Over the course of several weeks, increasing numbers of individual nanocrystals developed a positive charge. For CdS-capped nanocrystals, approximately 4 weeks after the sample was prepared, the relative fraction of nanocrystals with a permanent positive charge had increased such that about 50% had a positive charge, while the other 50% had remained neutral. Over the course of several months, this measurement was repeated four times on new samples with identical results; approximately 50% of the nanocrystals developed a positive charge over time. The magnitude of the charge was similar to the magnitude of the permanent charge on TOPO-capped nanocrystals. Thus, the positive charge on CdSe nanocrystals is not an intrinsic property but rather a function of sample history.

A very few nanocrystals (<1%), passivated with semiconductor or TOPO, exhibit a charge blinking behavior.[16] Since images are acquired line by line, we can observe blinking effects after a few lines, or equivalently, a few seconds with line scans of 1 Hz. Thus, our blinking temporal resolution is approximately a few seconds. The observed time scale for the on−off behavior ranges from seconds to minutes. The signal magnitude from one "on" period to another is approximately $Q_{on} \sim 0.5 \pm 0.05e$, while the off magnitude was $Q_{off} < 0.1e$. Since the observed charge blinking behavior contains nominally only one "on" value, this observation supports an assignment of this signal to one elementary charge. If this charge originates from a positive hole trapped on the nanocrystal surface, then the nanocrystal itself will be polarized to reduce the net electric field at the EFM tip. This screening by the nanocrystal, which will reduce the apparent magnitude of Q, is not considered in our model. We will subsequently refer to this positive signal as charge $Q = 1$.

EFM images of $\Delta\nu(2\omega)$ (dielectric image) of semiconductor-capped CdSe nanocrystals (see Figure 3b) were similar to corresponding images from TOPO-capped nanocrystals.[16] In the dielectric images, all nanocrystals had about the same signal magnitude. Since $\Delta\nu(2\omega)$ depends only on the dielectric constant of CdSe, the dielectric constants are similar, regardless of surface passivation.

In the single nanocrystal EFM measurements, it is necessary to use a PVB layer 1−2 nm thick to immobilize the particles. Use of the polymer has the disadvantage that the nanocrystal distance to the HOPG, and also to the tip, varies slightly from particle to particle. The roughness of the PVB insulator layer makes an accurate determination of ϵ from the raw $\Delta\nu(2\omega)$ signal over an individual nanocrystal difficult. Instead, ϵ was determined by using the (constant) $\Delta\nu(2\omega)$ magnitude over self-assembled nanocrystal islands without PVB layer. By fitting eq 2, we infer an absolute value of $\epsilon \sim 8$ for the static dielectric constant of a single nanocrystal. This value approximately agrees with predictions for a 5-nm CdSe nanocrystal, $\epsilon \sim 8.9$.[27] The uncertainty in ϵ is ±50% and arises almost exclusively from the large uncertainty in the spring constant of the EFM cantilever. The noise in the $\Delta\nu(2\omega)$ image is much less than ±10% and thus does not significantly affect our uncertainty in ϵ.

Permanent dipole moments, if present, would contribute to the $\Delta\nu(\omega)$ signal. Ensemble measurements have shown the presence of dipole moments, which scaled with CdSe nanocrystal size.[4,28] The dipole moment was on the order of 60−70 D for nanocrystals with a diameter of 4 nm.[4] If this dipole pointed directly toward the EFM tip, the resulting $\Delta\nu(\omega)$ signal would be comparable to that from a single positive charge. Measurements as a function of tip−sample separation could distinguish between charge and dipole fields. However, we currently do not have enough dynamic range to make that

measurement. As discussed above, we conclude that our $\Delta\nu(\omega)$ signals are from charges. For the three vastly different insulator and metallic substrates that we used, the observed signal is always zero or positive, as expected for one positive charge. These observations reflect EFM measurements of thousands of nanocrystals in total. We have never observed both negative and positive signals of varying intensity, as expected from a variable dipole orientation resulting from randomly oriented nanocrystals on the insulator surface. Also, when we observe a blinking in $\Delta\nu(\omega)$, the signal blinks on and off from nominally one value, as expected for a thermally induced charge-transfer process. A dipole resulting from positive and negative surface charges may be mobile and thus may always orient perpendicular to the HOPG surface along a static perpendicular field as to give a net positive signal. However, our EFM measurements are always performed whereby the static field between the tip and substrate is zero.

We conducted various experiments to explore the source of the permanent positive charge. Only those experiments that concerned exposure to light showed an effect. Exposure of a sample of individual nanocrystals on the metallic substrate for several hours to weak UV light with intensity $\sim 1\ \mu W/cm^2$ from a mercury−argon pen lamp resulted in a few positively charged nanocrystals out of approximately 25 in the given image. Two samples consisting of CdSe nanocrystals capped with CdS, which were prepared in the usual manner and which were stored in the dark, remained neutral for months after preparation. Also, the colloidal nanocrystal suspensions (CdS and ZnS capped) stored in the dark were initially neutral while the colloid (TOPO capped) stored in ambient lights was partially positively charged.

Other possible causes of permanent positive charge were investigated. A grounded EFM tip was touched to rafts of approximately 1000 nanocrystals, as well as to individual nanocrystals in an attempt remove or add charge. However, the nanocrystal charge was unchanged by this procedure. Oxidation of CdSe nanocrystals in air is known to occur over long periods of time.[10,29] We prepared a sample of individual CdSe nanocrystals, and stored it in an oxygen free environment under ambient light. Approximately 50% of the hundreds of nanocrystals we studied in this sample still developed a positive charge over time. Thus, oxidation is not related to nanocrystal charging. One might suggest that permanent charge may arise out of a very slow thermal equilibration between the Fermi levels of the initially neutral nanocrystal and the metallic substrate. However, as previously described, initially neutral samples stored in dark do not develop positive charge over many months.

B. Laser Excitation of Individual Nanocrystals. Excitation at 442 nm with an intensity $I \sim 20\ W/cm^2$ photoionizes ZnS-capped nanocrystals, as shown in Figure 3c,d. CdSe nanocrystals capped with CdS also photoionize under identical illumination conditions. At this excitation intensity, nanocrystals increase their charge by one positive charge. Thus, after photoionization an initially neutral nanocrystal exhibits $Q = 1$, and an initially charged nanocrystal exhibits $Q = 2$. Photoionization grows in over several minutes under continuous illumination. Individual nanocrystals on the PVB insulator all have slightly different environments and distances to the HOPG; most photoionize under continued irradiation, but some do not. We did not try to quantify the behavior of individual nanocrystals. Instead, we took a nominal ionization rise time to be the time at which the charge image remained unchanged for consecutive scans. For CdS-capped nanocrystals, this time was 5 to 10 min at an excitation intensity of $20\ W/cm^2$, which is similar to that of TOPO-capped nanocrystals.[16] The error in this measurement is roughly 3 min, which is half the time to acquire a complete image. ZnS-capped nanocrystals generally took factors of 3−4 longer to photoionize for a given excitation intensity. While photoexcitation of nanocrystals on HOPG, or on Au substrates with SAM layers, always resulted in photoionization, extended photoexcitation of nanocrystals on oxidized Si substrates did not increase their charge magnitude. However, signal-to-noise is poorer on Si substrates, and we did not quantitatively pursue this last observation.

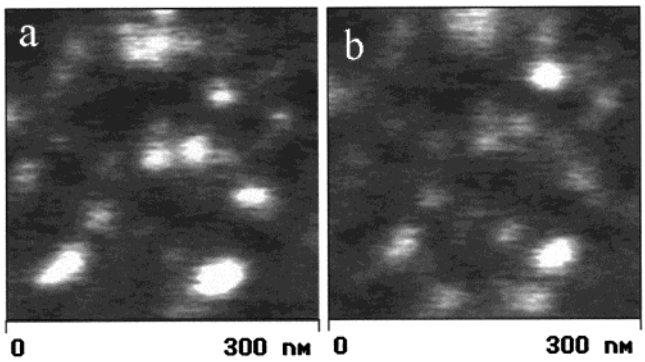

Figure 4. (a) EFM charge image of CdSe nanocrystals capped with TOPO after photoexcitation at 442 nm. The sample was prepared as in Figure 3. (c) EFM charge image approximately 30 min after the laser was extinguished. The sign of $\Delta\nu(\omega)$ in parts a and b is inverted for clarity.

If the continuous-wave laser excitation is stopped, then the photoionized charge decays as shown in Figure 4. In the 30 min between the images shown in parts a and b of Figure 4, a number of CdSe nanocrystals have lost their photoinduced charge, going from two to one positive charges. The time for most of the nanocrystals in a given image to return to their original charged state is on the order of 40−70 min. The spread in decay times arises from the effect of different local environments of the individual nanocrystals in a particular sample. In general, nanocrystals retained any permanent charge present before photoexcitation. Similar behavior was observed for all nanocrystals irrespective of surface passivation.

From all these results, we conclude that synthetic CdSe nanocrystals are largely neutral as prepared. However, after prolonged exposure to high or low intensity light, CdSe nanocrystals can develop and hold a positive charge, when examined in close proximity to a metal surface. Charge develops after irradiation either in solution or in close proximity to the metal.

C. Nanocrystal Monolayer Rafts. Quantitative ionization rate measurements as a function of excitation intensity were made on 2-D self-assembled aggregates of nanocrystals. These aggregates form on HOPG without an underlying polymer layer.[24] The capping TOPO layer itself provides a uniform, thin electrical insulation barrier of about 0.7 nm between the semiconductor core and the HOPG, and about 1.4 nm between nearest neighbors. The assembled nanocrystals form a single layer with a characteristic dimension of 100 nm, as shown in Figure 5a. A much smaller second layer sometimes is present on the first layer.

Upon 442 nm laser excitation, the magnitude of the $\Delta\nu(\omega)$ signal increased over time to a saturation level, as shown in Figure 5b−d. The charge signal did not monotonically increase nor did it remain constant at saturation. Rather, the $\Delta\nu(\omega)$ image exhibited a continuous blinking behavior whereby different sections of the image increased and/or decreased in magnitude over consecutive scans. These fluctuations only affected local signal intensities from one image to the next and thus did not

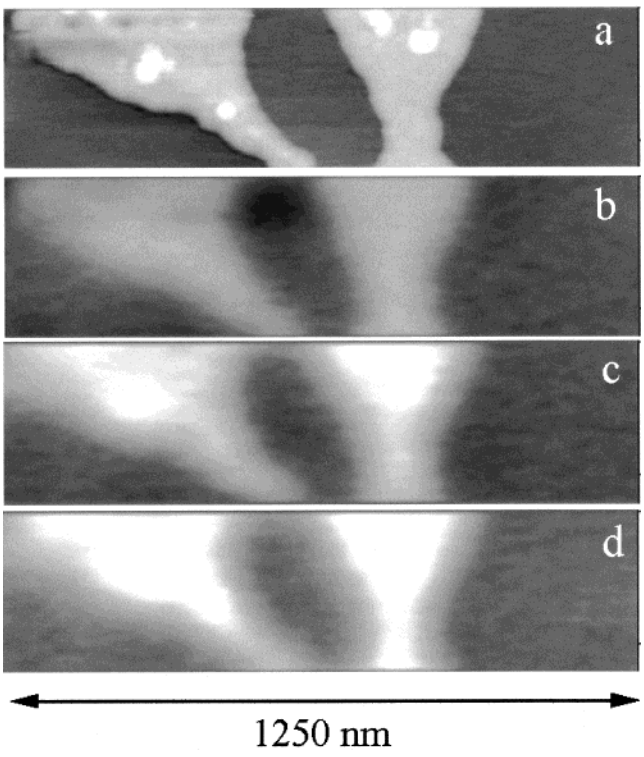

Figure 5. Tapping mode AFM (a) and EFM (b−d) charge images of CdSe nanocrystals with photoexcitation at 442 nm. Images were recorded after (b) 0 s, (c) 98 s, and (d) 588 s of photoexcitation. The excitation intensity was ~1.3 W/cm^2. The sign of $\Delta\nu(\omega)$ in parts b−d is inverted.

obscure the overall trend of an increasing signal with exposure time. The blinking behavior in the charge image has a rate similar to the rate of the blinking behavior observed in the charge images of single nanocrystals under photoexcitation. It is likely that the blinking results from electron transfer between the HOPG and the nanocrystals, since lateral charge motion between nanocrystals in the layer is slow on these time scales. These results were consistent among tens of nanocrystal rafts with various shapes and sizes, each of characteristic dimension 100 nm.

To obtain the $\Delta\nu(\omega)$ behavior under illumination, we averaged over the fluctuations. First, several line cuts were taken through a given $\Delta\nu(\omega)$ image. Then, the $\Delta\nu(\omega)$ signal from the points where the lines intersected the nanocrystals was recorded. Four to six values of $\Delta\nu(\omega)$ were recorded per image and averaged. We found that this adequately smoothed over the image-to-image fluctuations. Line cuts were taken through identical locations on consecutive images for consistency. For the sample whose charge images are shown in Figure 5, the average $\Delta\nu(\omega)$ as a function of exposure time is shown in Figure 6. The exposure time for a given image was taken to be the total exposure time exactly halfway through the acquisition of the image. The absolute magnitude of the $\Delta\nu(\omega)$ signal at saturation is $\Delta\nu(\omega) \sim 1.0 \pm 0.1$ Hz at a lift height of 30 nm. Within experimental error, this value is the same for all excitation intensities in the range from 0.1 to 2 W/cm^2.

The charge rise time and subsequent decay can be approximately modeled using a two-level formalism. Under photoexcitation, the rate of change of positive nanocrystals is given by

$$\frac{dp(t)}{dt} = \frac{\sigma I k}{h\nu} n(t) - K_n p(t) \qquad (8)$$

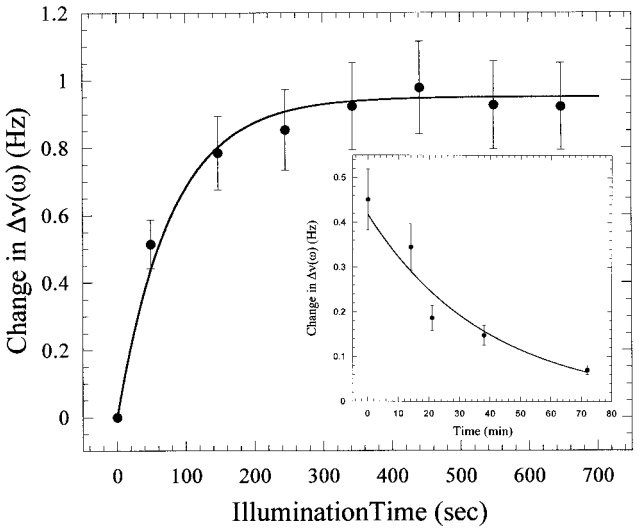

Figure 6. Absolute change in the magnitude of $\Delta\nu(\omega)$ as a function of photoexcitation time. The solid symbols are the measured data and the solid line is a theoretical fit based on a two-level rate equation model. The excitation intensity was ~1.3 W/cm^2. Insert: Decay of the magnitude of $\Delta\nu(\omega)$ after the excitation was removed. The excitation intensity was ~2 W/cm^2.

In the above equation, n and p are the percentage of nanocrystals that are neutral and positive, respectively, and I is the excitation intensity. $\sigma \sim 10^{-15}$ cm^2 is the absorption cross section per CdSe nanocrystal,[10] and k is the ionization probability per optical excitation. $K_n \sim 1/2400$ s^{-1} is the neutralization rate, which was determined from exponential fits to the charge signal decay after the laser illumination was extinguished (see inset to Figure 6). The rate of change of neutral nanocrystals, dn/dt, is equal to $-$dp/dt because $n + p = 1$. Since the data on individual nanocrystals indicate that approximately half of the nanocrystals have a positive charge before photoexcitation, $n(0) = p(0) = 0.5$. Our model is oversimplified in that it assumes that a single nanocrystal cannot contain more than one positive charge. Also, any effects of positively charged nanocrystals on the ionization rate of their neutral neighbors are also neglected.

The solution to eq 8 is an increasing exponential, which approaches

$$p(\infty) = \frac{\sigma I k}{h\nu} \Big/ \left(\frac{\sigma I k}{h\nu} + K_n\right) \qquad (9)$$

at long times. The ionization rate for a given intensity, $K_p = I\sigma k/h\nu$, was obtained by fitting the corresponding charge signal with the one adjustable parameter k. The solid line in Figure 6 is a best fit with $K_p = 0.012$ s^{-1}. The error in the average magnitude of $\Delta\nu(\omega)$ is ±10%, which results in an error of ±25% in the value of K_p.

The variation of the ionization rate with excitation intensity for TOPO-, CdS-, and ZnS-capped CdSe nanocrystals is shown in Figure 7. CdS- and TOPO-capped nanocrystals photoionize with similar rates. Quantitative agreement between the ionization rates of TOPO- and CdS-capped nanocrystals is consistent with our measurements of photoionization of individual nanocrystals and is also expected given the relative electron and hole band-offsets between CdSe and CdS, as will be discussed subsequently. On the other hand, at ~1.8 W/cm^2 excitation intensity ZnS-capped nanocrystals have ionization rates approximately four times lower than the CdS- or TOPO-capped nanocrystals. For excitation intensities at ~0.18 W/cm^2, we did not observe significant photoionization in ZnS-capped nanocrystals. These results are again in agreement with our single nanocrystal

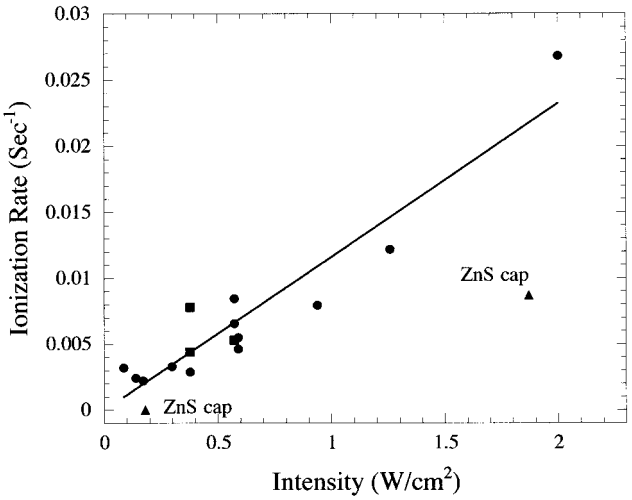

Figure 7. CdSe nanocrystal ionization rate versus photoexcitation intensity. The circles, squares, and triangles correspond to TOPO-, CdS-, and ZnS-capped nanocrystals, respectively. The solid line is a purely linear fit to the ionization rate of the TOPO-capped nanocrystals.

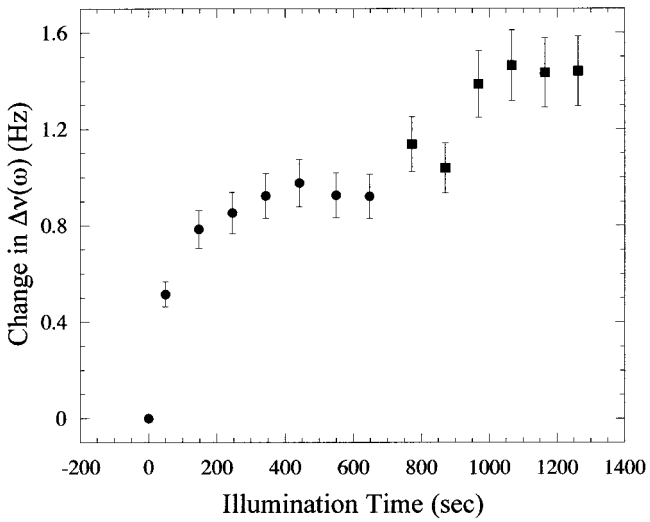

Figure 8. Absolute change in the magnitude of $\Delta\nu(\omega)$ as a function of photoexcitation time. The circles and squares correspond to low (1.3 W/cm^2) and high (20 W/cm^2) excitation intensities, respectively. High-intensity excitation began at $t = 686$ s after low-intensity excitation. The excitation wavelength for both intensities was 442 nm.

photoionization studies and also are expected given the relative electron and hole band-offsets between CdSe and ZnS.

Our simple two-level rate equation model assumes a linear dependence of the ionization rate on laser intensity. If photoionization is solely due to two-photon processes, such as Auger ionization, a square dependence is expected. We find good qualitative linear fits as shown in Figure 7. A purely quadratic fit is poor. From the slope, the average ionization probability per excitation is $k \sim 5 \times 10^{-6}$. The $\pm 60\%$ absolute error in this value is due to the error in tunneling time K_p as well as the error in determining the absolute excitation intensity at the sample. Note that the value of the ionization probability per excitation is the same order of magnitude as that observed in single nanocrystal luminescence blinking experiments.[10] These experiments also found a linear intensity dependence of photoexcitation leading to the nonluminescent dark state. In general, our present EFM experiments support the photoionization−recombination blinking mechanism advanced in earlier studies.

The magnitude of the saturated charge signal, which was approximately the same for all excitation intensities $I < 2$ W/cm^2, increased when the samples were exposed to higher laser intensities $I \sim 20$ W/cm^2. We observed this effect for tens of rafts on the five samples which were exposed to the higher excitation intensity, At the higher excitation intensities, the charge signal also eventually saturated, as shown in Figure 8. This result shows that at high excitation fluences CdSe nanocrystals can acquire more than one positive charge, which is also consistent with the high-intensity photoexcitation measurements of single nanocrystals. Detailed modeling of the multiionization is left for future studies.

Discussion

Positively charged CdSe nanocrystals are very well insulated by TOPO organic layers alone. Thus, if protected from light sources, on the HOPG, initially dark samples remain dark for months, while initially charged samples remain charged for months. No thermally induced charge equilibration between the nanocrystals and the metallic substrate occurs, even with only the thin 0.7 nm insulator (TOPO) present in the raft samples. In addition, charged nanocrystals cannot be discharged by touching with a grounded, metallic AFM tip.

In our surface photoionization experiments, the excited electron could directly tunnel into the HOPG, or it could transiently trap on the outside surface before transferring to the HOPG. Single visible photons do not have sufficient energy to directly photoionize nanocrystals in a vacuum. Sequential transfer of a surface trapped electron to the HOPG could occur by thermal tunneling or photon excitation. If photon assisted, then at least one step in this putative sequential two-photon process is saturated at our power levels, yielding an apparent linear intensity dependence.

The dependence upon shell properties in core/shell particles, observed in both raft and single nanocrystal experiments, supports the idea that the rate-limiting slow step involves electron tunneling across the semiconductor shell and not possible sequential transfer of a trapped electron on the outside of the shell to HOPG. In a TOPO-capped CdSe nanocrystal, the electron is far more delocalized than the hole, with a nonnegligible fraction of electron density on the nanocrystal surface.[30] For a semiconductor-capped nanocrystal, the electron wave function depends on the band off-sets of the semiconductor shell with respect to CdSe. For a CdS shell, the barrier height for the electron is so low that its wave function penetrates across the CdS.[22,31] However, the barrier to the hole is large and the hole is confined to the CdSe core. Therefore, CdS-capped nanocrystals should photoionize by losing an electron, with a time constant similar to that of TOPO-capped nanocrystals, as observed. For a ZnS shell, the barrier heights for both electron and hole are large.[22] While the electron and hole wave functions are expected to be well confined to the nanocrystal, the electron is still far more delocalized than the hole.[22] Consequently, for a ZnS shell, photoexcitation should also result in a positively charged nanocrystal, but photoionization should be more difficult than for CdS or TOPO, also as observed. Note that excitation at 780 nm, less than the CdSe nanocrystal band gap, did not cause photoionization. The average photoionization time seems to be extremely sensitive to the photoexcited electron barrier, while the hole barrier shows little effect.

The photoionization time depends on the distance to the HOPG as well as the electrical nature of the shell-capping material. Rafts, which are closer to the HOPG, show at least an order of magnitude faster charge rise time than individual particles stabilized by PVB, at the same laser intensity. Also, samples on 5 nm thick oxidized silicon showed no apparent

photoionization under the same time scale and intensity conditions as the HOPG experiments. These observations are consistent with direct tunneling. If a sequential process occurs, then sequential transfer to HOPG must compete with trapped electron back transfer to the hole. Further careful experiments are needed to definitively settle these questions.

The fact that our TOPO-capped nanocrystal solutions, stored in ambient light, show an immediate charge on the surface suggests that the photoexcited electron has been taken by a trace electron scavenger in solution. An alternate, and less likely possibility, is that the electron is loosely bound to the nanocrystal and transfers to the HOPG quickly before EFM data is obtained. In solution, surface passivation was recently shown to control depopulation of the electron from the lowest excited state.[32] In fact, recent ensemble measurements have indicated the presence of charged CdSe nanocrystals in the colloidal suspension.[4] However, in this case nanocrystal charging was attributed to thermal processes, and less than 1% of the nanocrystals were estimated to have a charge.

The nature of the observed positive charge on CdSe nanocrystals is not clear. The charge might be a delocalized mobile hole, or a trapped hole. A trapped hole can occur with or without a structural rearrangement of the nanocrystal. Surface trap states, with energy levels within the band-gap of the nanocrystal, are possible candidates, since they are likely to arise from Se dangling bonds,[31] which are most likely to ionize.[4]

We observed that in all samples that the nanocrystal polarizability was unchanged upon charging. We attempted to use this fact to extract information regarding the nature of the hole in a charged nanocrystal. We estimated an upper limit for the ac polarizability, at 800 Hz, of a mobile hole. For an ac voltage of $V_{ac} = 3$V and a tip−nanocrystal separation of 5 nm, the electric field at the nanocrystal center is $E \sim 4 \times 10^8$ V/m. The change in nanocrystal polarizability due to this one mobile hole is approximately $\Delta\epsilon \sim 0.07$ in a 5 nm nanocrystal. This value is too small with respect to the initial $\epsilon = 8$ value of a neutral nanocrystal for us to detect. Thus, we cannot infer information on the nature of the hole state from the $\Delta\nu(2\omega)$ data. However, we can say that, since the lifetime of the positive charge due to laser photoionization differs significantly from the infinite lifetime of the "permanent" positive charge, at least two types of charged states exist. Perhaps trapped holes can be further "permanently" stabilized by slow structural rearrangement.

All together, our measurements indicate that two classes of nanocrystals exist in a colloidal suspension, depending upon prior exposure to light: neutral and permanently photoionized, with the electron and hole likely well separated. Here we define photoionized to mean that, upon placement close to a metal surface, a nanocrystal exhibits a positive charge.

Conclusion

Through the use of electrostatic force microscopy, we have determined that CdSe nanocrystals are charge neutral as prepared. However, upon extended photoexcitation, a large percentage (>50%) photoionize and acquire a permanent, immobile positive elementary charge when examined by EFM. Ambient fluorescent lighting will photoionize CdSe nanocrystals given enough exposure time. EFM measurements of CdSe nanocrystals with different surface passivation illustrate the dependence of the photoionization rate on the electron surface confinement barrier. Measurements of the photoionization rate on graphite as a function of intensity suggest that the ionization occurs via a single photon, with probability $k \sim 5 \times 10^{-6}$ per excitation for TOPO passivation. The linear dependence of the ionization rate on laser intensity and the dependence of the ionization rate on electron confinement are both consistent with the hypothesis that ionization occurs by direct tunneling of the photoexcited electron into the metallic substrate. Direct proof of this tunneling theory requires further careful experiments. The dependence of charging on surface passivation observed here are similar those seen in photoconductivity of CdSe quantum dot solids, where charge separation appears to occur by direct tunneling between neighboring nanocrystals.[33]

The presence of a high number of photoionized nanocrystals in samples stored for some length of time helps to explain why many prior experiments have indicated the presence of static internal electric fields and dipoles. If the hole is trapped on the nanocrystal surface, then the polarized nanocrysal has a permanent dipole as well as a charge. Our observations directly support the photoionization mechanism for luminescence photodarkening in ensemble studies[34] and photoluminescence blinking in single nanocrystal luminescence. Control of photocharging will be essential for potential device application of nanocrystal materials.

Acknowledgment. We thank an anonymous referee for extensive and insightful comments on an earlier version of the manuscript. The authors also thank Professor Moungi Bawendi and Ken Shimitzu for providing ZnS-capped nanocrystals, Christopher Murray for assistance with synthesizing the CdS-capped nanocrystals, Zhonghua Yu and Guanglu Ge for sample preparation and CdSe synthesis, and Prof. George Flynn for the loan of equipment. We acknowledge the support of the Keck Foundation for the purchase of the AFM and Bell Laboratories for equipment donation. This research was supported under NSF MRSEC grant number DMR-98-09687 in the Center for Materials Research at Columbia University.

References and Notes

(1) Alivisatos, A. P. *J. Phys. Chem.* **1996**, *100*, 13226.
(2) Yoffe, A. D. *Adv. Phys.* **1993**, *42*, 173.
(3) Rabani, E.; Hetenyi, B.; Berne, B. J.; Brus, L. E. *J. Chem. Phys.* **1999**, *110*, 5355.
(4) Shim, M.; Guyot-Sionnest, P. *J. Chem. Phys.* **1999**, *111*, 6955.
(5) Nomura, S.; Kobayashi, T. *Phys. Rev. B* **1992**, *45*, 1305.
(6) Schmidt, M. E.; Blanton, S. A.; Hines, M. A.; Guyo-Sionnest, P. *J. Chem. Phys.* **1997**, *106*, 5254.
(7) Shiang, J. J.; Kadavanich, A. V.; Grubbs, R. K.; Alivisatos, A. P. *J. Phys. Chem.* **1995**, *99*, 17417.
(8) Empedocles, S. A.; Bawendi, M. G. *Science* **1997**, *278*, 2114.
(9) Empedocles, S.; Bawendi, M. *Acc. Chem. Res.* **1999**, *32*, 389.
(10) Nirmal, M.; Dabbousi, B. O.; Bawendi, M. G.; Macklin, J. J.; Trautman, J. K.; Harris, T. D.; Brus, L. E. *Nature* **1996**, *383*, 802.
(11) Nirmal, M.; Brus, L. *Acc. Chem. Res.* **1999**, *32*, 407.
(12) Efros, A. L.; Rosen, M. *Phys. Rev. Lett.* **1997**, *78*, 1110.
(13) Pistol, M. E.; Castrillo, P.; Hessman, D.; Prieto, J. A.; Samuelson, L. *Phys. Rev. B* **1999**, *59*, 10725.
(14) Mason, M. D.; Credo, G. M.; Weston, K. D.; Buratto, S. K. *Phys. Rev. Lett.* **1998**, *80*, 5405.
(15) Bertram, D.; Hanna, M. C.; Nozik, A. J. *Appl. Phys. Lett.* **1999**, *74*, 2666.
(16) Krauss, T. D.; Brus, L. E. *Phys. Rev. Lett.* **1999**, *83*, 4840.
(17) Martin, Y.; Abraham, D. W.; Wickramasinghe, H. K. *Appl. Phys. Lett.* **1988**, *52*, 1103.
(18) Terris, B. D.; Stern, J. E.; Rugar, D.; Mamin, H. J. *Phys. Rev. Lett.* **1989**, *63*, 2669.
(19) Martin, Y.; Williams, C. C.; Wickramasinghe, H. K. *J. Appl. Phys.* **1987**, *61*, 4723.
(20) Murray, C. B.; Norris, D. J.; Bawendi, M. G. *J. Am. Chem. Soc.* **1993**, *115*, 8706.
(21) Hines, M. A.; GnyotSionnest, P. *J. Phys. Chem.* **1996**, *100*, 468.
(22) Dabbousi, B. O.; RodriguezViejo, J.; Mikulec, F. V.; Heine, J. R.;

Mattoussi, H.; Ober, R.; Jensen, K. F.; Bawendi, M. G. *J. Phys. Chem. B* **1997**, *101*, 9463.

(23) Peng, X. G.; Schlamp, M. C.; Kadavanich, A. V.; Alivisatos, A. P. *J. Am. Chem. Soc.* **1997**, *119*, 7019.

(24) Ge, G.; Brus, L. E. *J. Phys. Chem. B* **2000**, *104*, 9573.

(25) MESP Cantilevers from Digital-Instruments-Veeco Metrology Group.

(26) Belaidi, S.; Girard, P.; Leveque, G. *J. Appl. Phys.* **1997**, *81*, 1023.

(27) Wang, L. W.; Zunger, A. *Phys. Rev. B* **1996**, *53*, 9579.

(28) Blanton, S. A.; Leheny, R. L.; Hines, M. A.; GuyotSionnest, P. *Phys. Rev. Lett.* **1997**, *79*, 865.

(29) Katari, J. E. B.; Colvin, V. L.; Alivisatos, A. P. *J. Phys. Chem.* **1994**, *98*, 4109.

(30) Schooss, D.; Mews, A.; Eychmuller, A.; Weller, H. *Phys. Rev. B* **1994**, *49*, 17072.

(31) Pokrant, S.; Whaley, K. B. *Eur. Phys. J. D* **1999**, *6*, 255.

(32) Klimov, V. I.; McBranch, D. W.; Leatherdale, C. A.; Bawendi, M. G. *Phys. Rev. B* **1999**, *60*, 13740.

(33) Leatherdale, C. A.; Kagan, C. R.; Morgan, N. Y.; Empedocles, S. A.; Kastner, M. A.; Bawendi, M. G. *Phys. Rev. B* B **2000**, *62*, 2669.

(34) Rodriguez-Viejo, J.; Mattoussi, H.; Heine, J. R.; Kuno, M. K.; Michel, J.; Bawendi, M. G.; Jensen, K. F. *J. Appl. Phys.* **2000**, *87* 8526.